Ann. Geophysicae 9, 641–647 (1991)

Annales Geophysicae

Linear impact of thermal inhomogeneities on mesoscale atmospheric flow with zero synoptic wind *

G. A. Dalu [1,6], R. A. Pielke [2], R. Avissar [3], G. Kallos [4], M. Baldi [2,5], A. Guerrini [5]

[1] G. A. Dalu, Cooperative Institute for Research in the Atmosphere, CIRA-CSU, Foothill Campus, Fort Collins, CO 80523, USA
[2] Department of Atmospheric Science, CSU, Foothill Campus, Fort Collins, CO 80523, USA
[3] Department of Meteorology and Physical Oceanography, Cook College, Rutgers University, New Brunswick, NJ, USA
[4] Department of Applied Physics, University of Athens, Ippocratous 33, Athens, Greece 10680
[5] Area Ricerca Frascati, ARF-CNR, Via G. Galilei, CP 27, Frascati-Rome, Italy 00044
[6] Institute for Atmospheric Physics, IFA-CNR, P.le L. Sturzo 31, Rome, Italy 00144

Received December 6, 1990; revised May 28, 1991; accepted July 12, 1991

Abstract. In this paper we present an analytical evaluation of the perturbations to mesoscale atmospheric flows induced by thermal inhomogeneities in the convective boundary layer. We study the time evolution of these perturbations as a function of the intensity and of the horizontal and vertical scales of the diabatic forcing. The problem is approached using Laplace transform theory for the time behavior and Green function theory for the spatial structure. Results show that the growth of the atmospheric perturbations closely follows the growth of the convective boundary layer; the transient being characterized by a number of inertia-gravity oscillations of decreasing intensity. The vertical scale is determined by the depth of the convective boundary layer; and the horizontal scale is determined by the local Rossby deformation radius. Sinusoidally periodic thermal forcing induce periodic atmospheric cells of the same horizontal scale. The intensity of mesoscale cells increases for increasing values of the wave number, reaches its maximum value when the wavelength of the forcing is of the order of the local Rossby radius, and then decreases as the wavelength of the forcing decreases. However, because of the destructive interference between mesoscale cells, the intensity of the vertical velocity is only a weak function of the wave numbers, for large wave numbers. Periodic square wave surface thermal inhomogeneities are more effective than sinusoidal waves in generating mesoscale cells, i.e. the intensity of the flow is generally stronger.

Introduction

Subgrid-scale parameterization is of considerable importance in regional and larger scale models because these models seldom have more than few grid points within a Rossby radius, yet the mesoscale flow driven by thermal horizontal inhomogeneities in the *Convective Boundary Layer* (CBL) may be significant. Therefore mesoscale effects need to be introduced in parametric form into those large scale models.

Terrain in the real world is almost never uniform: for instance, in natural areas there may be a variety of vegetation types and patches of vegetated or unvegetated areas which can modify the mesoscale atmospheric flow. Horizontal thermal inhomogeneities in the planetary boundary layer are a well known source of mesoscale circulation systems. Thermally-forced mesoscale systems such as land and sea breezes, mountain-valley winds, and urban heat island circulations have been the subject of many studies (e.g., see references in Pielke, 1984, and Pielke and Segal, 1986). Some thermally-generated mesoscale circulations are due to horizontal inhomogeneities in ground wetness, vegetation cover, snow cover, cloud cover, etc. (e.g. Zhang and Anthes, 1982; Garrett, 1982; Yan and Anthes, 1988; Segal *et al.*, 1988). In addition, there are also anthropogenic modifications of soil and vegetation, such as irrigated or non-irrigated fields, crops at different stages of development, inhabited areas, etc. (Hanna and Swisher, 1971; Anthes, 1984; Segal *et al.*, 1984; Segal *et al.*, 1989). Such thermal inhomogeneities may extend from few square meters to hundreds or even thousands of square kilometers (Wetzel and Chang, 1988). A number of observational, numerical, and analytical studies have been made of these physiographically forced circulations (Abbs and Pielke, 1986; Mahfouf *et al.*, 1987; Mahrer and Pielke, 1977; McCumber and Pielke, 1981; Zhang and Anthes, 1982; Yan and Anthes, 1988).

Since the fine horizontal structure of the terrain thermal inhomogeneities is not usually resolved in regional and large scale non-linear numerical models, it is important to give an analytical quantitative evaluation of their impact on the atmospheric flow. In this paper, we present an analytical theory for resolving the atmospheric perturbation and for evaluating the vertical velocities, resulting from thermal inhomogeneities in the absence of large

* Paper presented at the workshop W 11.5 on "Physical, chemical and biological processes in the atmospheric boundary layer", EGS General Assembly, Copenhagen 23–27 April, 1990

scale flow (or in presence of very weak large scale flow) in the limit of a linear theory.

Governing equation and evolution of the horizontal and vertical scales

From Rotunno (1983) and Dalu and Pielke (1989) the linearized two-dimensional primitive equations describing thermally-forced atmospheric flow, in the absence of a large-scale wind, can be reduced to a single equation for the streamfunction:

$$\left[\left(\frac{\partial}{\partial t}+\lambda\right)^2+N^2\right]\frac{\partial^2}{\partial x^2}\psi+\left[\left(\frac{\partial}{\partial t}+\lambda\right)^2+f^2\right]\frac{\partial}{\partial z^2}\psi = -\frac{\partial}{\partial x}Q. \tag{1}$$

where f is the Coriolis parameter, N is the Brunt-Väisälä frequency, and λ^{-1} is the damping time due to friction, i.e. the persistency of the mesoscale flow when the diabatic forcing vanishes. In this paper we use the following values for these parameters:

$$N=10^{-2}\,\mathrm{s}^{-1};\quad f=2\omega\sin\alpha=O(10^{-4})\,\mathrm{s}^{-1};$$
$$\lambda=O(\omega);\quad \omega=\frac{2\pi}{\mathrm{day}}. \tag{2}$$

Q is the diabatic buoyancy source,

$$Q=\frac{g}{\varrho\, c_p\,\bar{\Theta}}\frac{F_0\, r(x)\, q(t)}{h}\,He(h-z)=Q_0\, r(x)\, q(t)\,He(h-z) \tag{3}$$

uniformly distributed through the depth h of the CBL, as indicated by the Heaviside function He in Eq. (3). $F_0\, r(x)\, q(t)$ is the heat flux at the ground, which has a horizontal distribution $r(x)$ and a time behavior $q(t)$.

Non-dimensional time variables

We first define the characteristic time scale of the system T, and we use it to non-dimensionalize time:

$$T=\frac{1}{\sqrt{f^2+\lambda^2}}=O(10^4)\,\mathrm{s}\qquad \tau=t\,\mathrm{T}^{-1}; \tag{4}$$

T decreases with increasing latitude and friction (friction keeps the time scale T finite at the equator). We introduce the Laplace transform, defined as

$$\hat{f}(s)=L\{f(\tau)\}=\int_0^\infty f(\tau)\exp(-s\,\tau)\,\mathrm{d}\tau \quad \text{and}$$
$$LL^{-1}\{f(\tau)\}=f(\tau).$$

We recall also that:

$$f(\tau\to\infty)=\lim_{s\to 0} s\hat{f}(s) \tag{5}$$

i.e. $f(\tau)\approx s\hat{f}(s)$

when $s\ll 1$ and $\tau=\tau_0\gg 1 \Rightarrow t=t_0\gg T.$ (6)

t_0 is the time when an almost stationary state is reached; t_0 is larger than the characteristic response time, T, of the system.

Evolution of the vertical and horizontal scales, and the non-dimensional coordinates

We recall the relation between Q and h (Green and Dalu, 1980):

$$r(x)\,h(t)=r(x)\frac{2Q_0}{N^2}\int_0^t \mathrm{d}t'\,q(t');\quad h_0=\frac{2Q_0}{N^2}\int_0^{t_0}\mathrm{d}t'\,q(t'). \tag{7}$$

The Laplace transforms of the CBL height, $\hat{h}$ and the non-dimensional vertical coordinate, $\hat{\eta}$, are:

$$\hat{h}=h_0\frac{\hat{q}(s)}{s};\quad \hat{\eta}=\frac{z}{\hat{h}}. \tag{8}$$

The Laplace transforms of the horizontal scale, $\hat{R}$, and the non-dimensional horizontal coordinate, $\hat{\xi}$, are:

$$\hat{R}=\hat{h}\left(\frac{\tilde{N}^2+p^2}{\hat{f}^2+p^2}\right)^{1/2}\approx\hat{h}\frac{\tilde{N}}{\sqrt{\hat{f}^2+p^2}};\quad p=s+\lambda;\quad \hat{\xi}=\frac{x}{\hat{R}} \tag{9}$$

The horizontal scale evolves in time as:

$$R(t)=R_0\int_0^t\frac{\mathrm{d}t'}{T}\frac{h(t-t')}{h_0}\exp(-\lambda t')\,J_0(f t');$$
$$R_0=h_0\frac{N}{\sqrt{f^2+\lambda^2}}. \tag{10}$$

Friction acts to reduce the horizontal scale R_0 (the Rossby radius) and exponentially damps the intertial oscillations described by the Bessel function, which provides some damping even without friction, Eq. (10).

The evolutions of $h(t)$ and $R(t)$ are shown in Fig. 1 a for a sinusoidal in time thermal forcing, and Fig. 1 b for an impulsive thermal forcing; for different values of friction. In both cases, the growing time of the boundary layer is about half a day, $t_0\approx$ day. R grows, as the convective boundary develops, through inertia-gravity oscillations. The relative amplitude of these waves is $O[\exp(-\lambda t)\,J_0(f t)]$; i.e. the inertia-gravity oscillations decay as a Bessel function or faster (exponentially) in the presence of friction, and their amplitude is usually negligible when $t\geq t_0\approx 0.5$ day.

Local Rossby radius

When two adjacent regions both experience a warming of similar intensity, Q in Eq. (3), is given by

$$Q=Q_0\,q(t)\,[He(x)+(1-\gamma)\,He(-x)]\,He(h_0-z), \tag{11}$$

with $\gamma<O(1)$, indicating that the two regions have similar heating; then the difference in N^2 between the two regions is of the order or

$$N_\gamma^2=|\gamma|\,N^2. \tag{12}$$

R_0 has been replaced by its local value, R_{0_γ}, equal to

$$R_{0_\gamma}=h_0\left(\frac{N_\gamma^2+\lambda^2}{f^2+\lambda^2}\right)^{1/2}\approx h_0\frac{N_\gamma}{\sqrt{f^2+\lambda^2}}. \tag{13}$$

Because of the reduction of N^2 (Eq. 12), the horizontal scale (Eq. 13) is correspondingly reduced, while the vertical scale remains of the order of $h(t)$. The aspect ratio

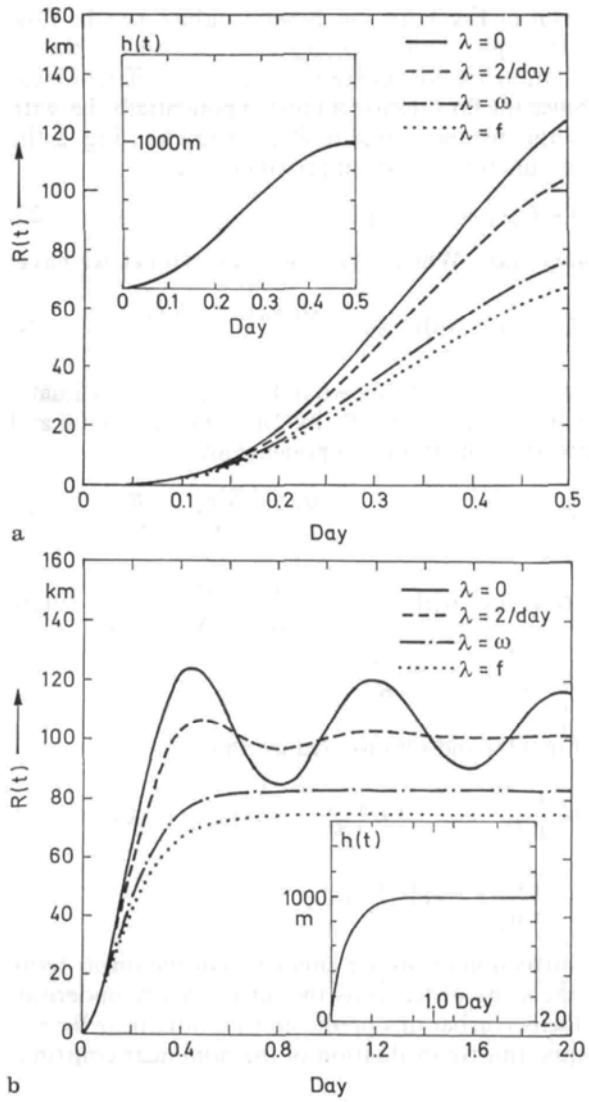

Fig. 1 a, b. The evolution of the Rossby radius for different values of friction: **a** for a sinusoidal forcing; $h(t) = h_0(1-\cos\omega t)/2$ is given in the insert; **b** for a convective boundary layer asymptotically growing to h_0; $h(t) = h_0(1-\exp(-t/t_0)$ is given in the insert

becomes:

$$A = \left(\frac{f^2+\lambda^2}{N_\gamma^2+\lambda^2}\right)^{1/2}.$$

Atmospheric cells, generated by thermal inhomogeneities having a wavelength smaller than twice R_{0_γ}, will interact with each other.

Non-dimensional equation for the streamfunction

Using the definitions stated above, the streamfunction Eq. (1) can be written as:

$$\frac{\partial^2}{\partial\hat{\xi}^2}\hat{\psi} + \frac{\partial^2}{\partial\hat{\eta}^2}\hat{\psi} = -\hat{\beta}(p)\frac{\partial}{\partial\hat{\xi}}\hat{Q}, \tag{14}$$

$$\hat{\beta}(p) = \left(\frac{1}{\tilde{N}^2+p^2}\right)^{1/2}\left(\frac{1}{\tilde{f}^2+p^2}\right)^{1/2} \approx \frac{1}{\tilde{N}}\frac{1}{\sqrt{\tilde{f}^2+p^2}}. \tag{15}$$

The variables with the tilde are non-dimensional; the variables with the hat are their Laplace transforms.

Boundary conditions and Green functions

We assume that the terrain is flat and that the vertical velocity vanishes at the ground:

$$w(x, z=0, t) = \tilde{w}(\hat{\xi}, \hat{\eta}=0, \tau) = \hat{w}(\hat{\xi}, \hat{\eta}=0, s) = 0. \tag{16}$$

When the operator in Eq. (14) is elliptic, the Green function is:

$$\hat{g}_\psi = -\frac{1}{2\pi}\ln\left[\frac{(\hat{\xi}-\hat{\xi}')^2+(\hat{\eta}+\hat{\eta}')^2}{(\hat{\xi}-\hat{\xi}')^2+(\hat{\eta}-\hat{\eta}')^2}\right]^{1/2}. \tag{17}$$

The perturbation is trapped, i.e. vanishes at ∞:

$$\hat{w}(\hat{\xi}=\infty, \hat{\eta}=\infty, s) = 0. \tag{18}$$

When the operator in Eq. (14) is hyperbolic, the Green function is:

$$\hat{g}_\psi = \tfrac{1}{2}[He(\hat{\eta}-\hat{\eta}'-|\hat{\xi}-\hat{\xi}'|) - He(\hat{\eta}+\hat{\eta}'-|\hat{\xi}-\hat{\xi}'|)]. \tag{19}$$

The perturbation is a propagating wave.

Important note. When the operator is elliptic, the intensity of the perturbation decays as the logarithm of the ratio between distance from the source $(\hat{\xi}', \hat{\eta}')$ and from its mirror image $(\hat{\xi}', -\hat{\eta}')$, Eq. (17) (the perturbation is confined in the neighborhood of the source and of its image). The presence of poles in inverting the solution in the transformed space, gives propagating inertia-gravity waves vanishing at ∞ in the physical space; the related solutions are in terms of Bessel and trigonometric functions (Dalu and Pielke, 1989).

The case when the operator becomes hyperbolic (non-vanishing propagating waves) under sinusoidal forcing has been treated by Rotunno (1983), and by Dalu and Pielke (1989). Furthermore, Sun and Orlanski (1981) have shown that some modes can become unstable for some values of the pulsation and the wave number.

Atmospheric response

The atmospheric response is given by the inverse Laplace transform of

$$\hat{\psi} = \tilde{Q}_0\,\hat{q}(s)\,\hat{\beta}(p)\,\hat{H}_\psi(\hat{\xi}, \hat{\eta}); \quad \hat{u} = \tilde{Q}_0\,\hat{q}(s)\,\hat{\beta}(p)\,\hat{H}_u(\hat{\xi}, \hat{\eta});$$
$$\hat{w} = \tilde{Q}_0\,\hat{q}(s)\,\hat{\beta}(p)\,\hat{H}_w(\hat{\xi}, \hat{\eta});$$

$$\hat{v} = -\frac{\tilde{f}}{p}\hat{u}; \quad \hat{b} = \frac{1}{p}[\hat{Q} - N^2\hat{w}] \tag{20}$$

where

$$\hat{G}(\hat{\xi}-\hat{\xi}', \hat{\eta}) = \int_0^{\hat{h}} d\hat{\eta}'\,\hat{g}(\hat{\xi}-\hat{\xi}', \hat{\eta}-\hat{\eta}').$$

The integration limit, $\hat{h}$, is the Laplace transform of h. In addition,

$$\hat{H}(\hat{\xi}, \hat{\eta}) = \int_b d\hat{\xi}'\,\hat{G}(\hat{\xi}-\hat{\xi}', \hat{\eta})\frac{\partial\hat{r}(\hat{\xi}')}{\partial\hat{\xi}'}.$$

D is the horizontal region with non-zero forcing. When D is finite, $\hat{H}$ can be written also as:

$$\hat{H}(\hat{\xi},\hat{\eta}) = -\int_D \mathrm{d}\hat{\xi}'\,\hat{r}(\hat{\xi}')\,\frac{\partial}{\partial\hat{\xi}'}\,\hat{G}(\hat{\xi}-\hat{\xi}',\hat{\eta}),$$

where:

$$\hat{G}_u(\hat{\xi},\hat{\eta}) = \frac{1}{2\pi}\ln\left\{\frac{[\hat{\xi}^2+(\hat{\eta}+1)^2]^{1/2}\,[\hat{\xi}^2+(\hat{\eta}-1)^2]^{1/2}}{[\hat{\xi}^2+\hat{\eta}^2]}\right\},$$

$$\hat{G}_w(\hat{\xi},\hat{\eta}) = -\frac{1}{2\pi}\left[\tan^{-1}\left(\frac{\hat{\eta}+1}{\hat{\xi}}\right)-2\tan^{-1}\left(\frac{\hat{\eta}}{\hat{\xi}}\right)+\tan^{-1}\left(\frac{\hat{\eta}-1}{\hat{\xi}}\right)\right],$$

$$\hat{G}_\psi(\hat{\xi},\hat{\eta}) = \frac{1}{2\pi}\left\{\xi\left[\tan^{-1}\left(\frac{\hat{\eta}+1}{\hat{\xi}}\right)-2\tan^{-1}\left(\frac{\hat{\eta}}{\hat{\xi}}\right)+\tan^{-1}\left(\frac{\hat{\eta}-1}{\hat{\xi}}\right)\right]+(\hat{\eta}+1)\ln[\hat{\xi}'+(\hat{\eta}+1)^2]^{1/2}-2\hat{\eta}\ln[\hat{\xi}^2+\hat{\eta}^2]^{1/2}+(\hat{\eta}-1)\ln[\hat{\xi}^2+(\hat{\eta}-1)^2]^{1/2}\right\}. \quad (21)$$

In physical units we have:

$$\psi(x,z,t) = \frac{Q_0 h_0}{TN} \cdot \{q(t) * \{\exp(-\lambda t)\cdot\{J_0(ft) * H_\psi(x,z,t)\}\}\}, \quad (22)$$

where $\{*\}$ denotes the convolution product in time. The time-dependent transfer functions can be written in terms of Bessel functions, trigonometric functions, and exponentials (see Dalu and Pielke, 1989). The time evolution is then reconstructed through the use of the Faltung theorem (Fodor, 1965). The resulting behavior is similar to the one shown in Fig. 1 for the Rossby radius; i.e. the flow evolves through a series of damped inertial-gravity waves, the oscillation are not generally in-phase at different locations. Since the flow decays almost exponentially, i.e. with an e-folding distance equal to R_0, as shown in Fig. 2, the structure function can be approximated as:

$$\hat{G}_\psi(\hat{\xi},\hat{\eta}) \approx \hat{G}_\psi(\hat{\xi}=0,\hat{\eta})\exp(-|\hat{\xi}|). \quad (23)$$

Stationary state. When $t \gtrsim t_0$ and $r(x) = He(x)$, we have:

$$\psi = \psi_0\, G_\psi(\xi,\eta) \quad \text{with} \quad \psi_0 = \frac{Q_0 h_0 t_0}{N} = \frac{N h_0^2}{2}. \quad (24)$$

The flow from Eq. (24), shown in Fig. 3a, is approximately contained in a region $2R_0$ by $2h_0$. The horizontal and the vertical momentum components are:

$$u = u_0\, G_u(\xi,\eta) \quad \text{with} \quad u_0 = \frac{\psi_0}{h_0} = \frac{N h_0}{2} = \frac{R_0}{2T} \quad (25)$$

$$w = w_0\, G_w(\xi,\eta) \quad \text{with} \quad w_0 = u_0\,\frac{h_0}{R_0} = \frac{\psi_0}{R_0} = \frac{h_0}{2T} \quad (26)$$

$$\text{with} \quad \eta = \frac{z}{\eta_0}; \quad \xi = \frac{x}{R_0}.$$

From Eqs. (25) and (26) we deduce that:

$$\frac{\partial}{\partial t} = O\left(\frac{1}{T}\right); \quad u\frac{\partial}{\partial x} = O\left(\frac{u_0}{R_0}\right) = O\left(\frac{1}{2T}\right) \quad \text{and}$$

$$w\frac{\partial}{\partial z} = O\left(\frac{w_0}{h_0}\right) = O\left(\frac{1}{2T}\right)$$

i.e. the advection terms are smaller than the linear term, but of the same order; thus the linear theory underestimates the perturbations predicted by a nonlinear theory. For a quantitative evaluation of the nonlinear contribu-

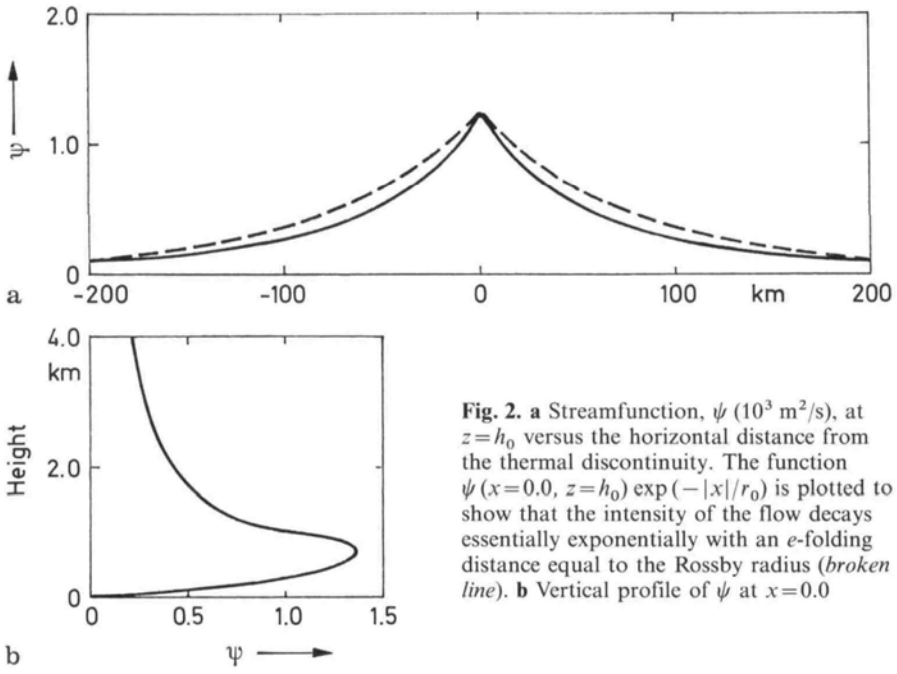

Fig. 2. a Streamfunction, ψ (10^3 m^2/s), at $z=h_0$ versus the horizontal distance from the thermal discontinuity. The function $\psi(x=0.0,\, z=h_0)\exp(-|x|/r_0)$ is plotted to show that the intensity of the flow decays essentially exponentially with an e-folding distance equal to the Rossby radius (*broken line*). **b** Vertical profile of ψ at $x=0.0$

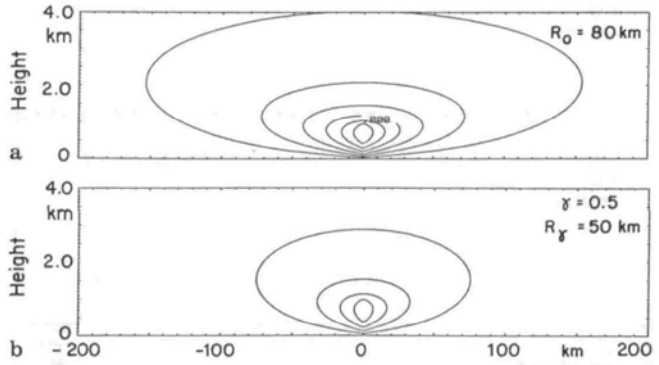

Fig. 3. a Streamfunction isolines for a discontinuous change of heat flux at $x=0.0$ at 40° of latitude ($\lambda=\omega$); $h_0=1000$ m, $\Delta\psi=0.2$ (10^3 m^2/s). **b** Streamfunction isolines when one region experiences a heat flux 50% less intense than the adjacent region, i.e. $\gamma=0.5$

tion see the paper by Pielke *et al.* (1991). The along-front momentum component is:

$$v \approx -\frac{t_0}{2} f u. \tag{27}$$

The temperature perturbation is:

$$\theta = He(x)\, He(h_0-z)(h_0-z)\,\Theta_z - [He(-x)+He(x)\,He(z-h_0)]\,\Delta_z\,\Theta_z. \tag{28}$$

Here we refer to heated land but the temperature perturbation will be positive whenever a CBL occurs due to superdiabatic lapse rate at the surface (e.q. over warm water patches also). Δ_z is the vertical displacement of the air parcels:

$$\Delta_z(x,z,t_0) \approx \frac{t_0}{2} w(x,z,t_0).$$

When the flow results from adjacent differentially heated regions in Eq. (11), the intensity of the mesoscale flow reduces to:

$$\psi_{0_\gamma} = \gamma \psi_0. \tag{29}$$

The flow intensity is proportional to γ. If we set the threshold for the generation of significant mesoscale flow at 20%, the influence of the mesoscale flow need to be included (explicitly or in parametric form) when:

$$\frac{\psi_{0_\gamma}}{\psi_0} > 0.20 \Rightarrow \gamma > 0.20.$$

We will refer to this measure as the resolution threshold suggesting that, for $\gamma<0.2$, the influence of the spatial heterogenity can be ignored. The flow shown in Fig. 3 b refers to the case when $\gamma=0.5$ in Eq. (11), i.e. the upstream region experiences 50% less heat than downstream of the thermal discontinuity. The mesoscale flow shown in Fig. 3 b is less intense (from Eq. (13)), and is less extensive than the flow shown in Fig. 3 a.

Atmospheric response to periodic thermal forcing

Throughout this section, in evaluating the averages and the convolution integrals along the horizontal coordinate we make use of the fact that the intensity of the flow decays exponentially with an *e*-folding distance equal to R_0 (Fig. 2):

$$\psi = \psi_0\, g(z) \exp\left(-\frac{|x|}{R_0}\right) \qquad w = -\frac{\partial\psi}{\partial x} \tag{30}$$

$$g(z) = G_\psi(x=0.0,z) = \frac{1}{2\pi}\frac{z}{h_0}\ln\left|\frac{z^2-h_0^2}{z^2}\right| + \frac{1}{2\pi}\ln\left|\frac{z+h_0}{z-h_0}\right|.$$

When the diabatic heating is sinusoidally periodic over the entire horizontal domain, with L_m as wavelength:

$$Q = Q_0\, q(t)\, He(h-z)\left[\frac{1}{2}+\frac{1}{2}\sin\left(\frac{m\pi x}{R_0}\right)\right]; \quad m=\frac{2R_0}{L_m}, \tag{31}$$

then the streamfunction is given by,

$$\psi = \frac{\psi_0}{2}\int_{-\infty}^{\infty}\frac{m\pi\,dx'}{R_0}\cos\left(\frac{m\pi(x-x')}{R_0}\right)G_\psi(x',z) = \psi_0\, g(z)\frac{m\pi}{(m\pi)^2+1}\cos\left(\frac{m\pi x}{R_0}\right). \tag{32}$$

Here m is the number of wavelengths in a $2R_0$ distance (m need not be an integer). If we set the resolution threshold at 0.20:

$$\frac{\psi_{0_m}}{\psi_0} > 0.20 \Rightarrow \frac{m\pi}{(m\pi)^2+1} > 0.20 \Rightarrow 0.4 < m < 1.2.$$

Thus the mesoscale flow need to be included (explicitly or in parametric form) when $0.4<m<1.2$. The intensity of the atmospheric response as a function of m is shown in Fig. 4 a. The intensity of the mesoscale cells decreases monotonically for m large (shown in Fig. 5). The vertical velocity is:

$$w = -\frac{\partial\psi}{\partial x} = w_0\, g(z)\frac{(m\pi)^2}{(m\pi)^2+1}\sin\left(\frac{m\pi x}{R_0}\right). \tag{33}$$

When $m>1$, the vertical velocity is a weak function of m (Fig. 4 c). When the forcing is a periodic square wave over the entire horizontal domain, with L_m as wavelength:

$$Q = Q_0\, q(t)\, He(h-z)\left[\frac{1}{2}+\frac{1}{2}\sum_{n=1,3\ldots}^{\infty}\frac{4}{n\pi}\sin\left(\frac{mn\pi x}{R_0}\right)\right]; \quad m=\frac{2R_0}{L_m}, \tag{34}$$

then the streamfunction is given by

$$\psi = \psi_0\, g(z)\sum_{n=1,3\ldots}^{\infty}\frac{4}{n\pi}\frac{mn\pi}{(mn\pi)^2+1}\cos\left(\frac{mn\pi x}{R_0}\right). \tag{35}$$

If we set the resolution at 0.20:

$$\frac{\psi_{0_m}}{\psi_0} > 0.20 \Rightarrow \sum_{n=1,3\ldots}^{\infty}\frac{4}{n\pi}\frac{mn\pi}{(mn\pi)^2+1} > 0.20 \Rightarrow 0.05 < m < 2.2.$$

Thus, for square heating patches, the mesoscale flow needs to be included (explicitly or in parametric form)

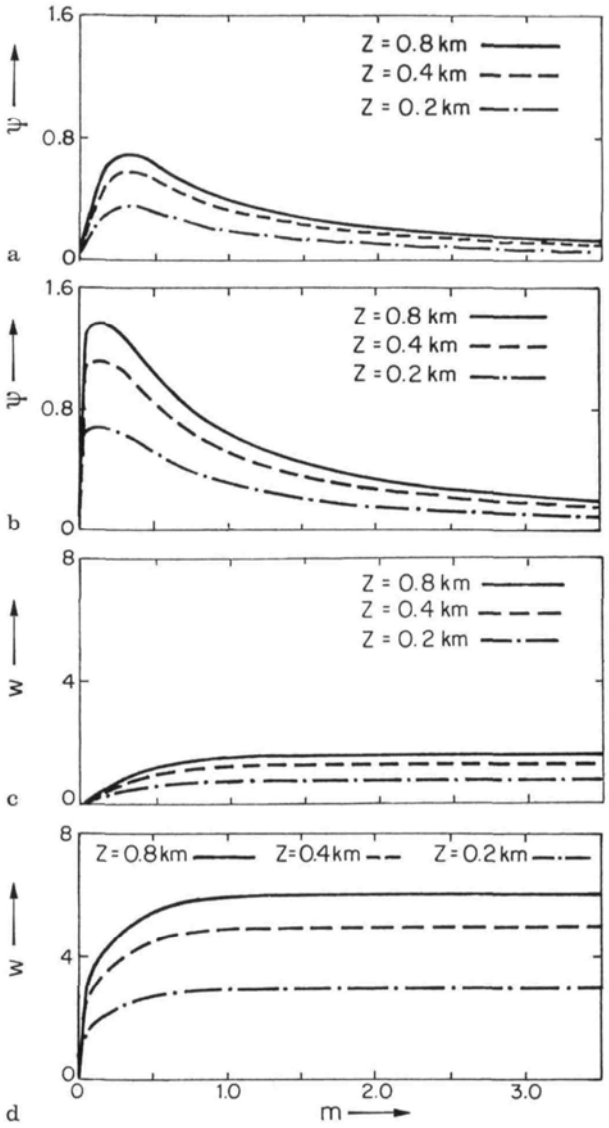

Fig. 4. **a** Intensity of the flow, induced by a sinusoidal periodic forcing, versus horizontal wave number; **b** same as **a** but for a periodic square wave; **c** vertical velocity for a sinusoidal periodic forcing; **d** vertical velocity for a periodic square wave; **e** average vertical mesoscale heat flux for a sinusoidal periodic forcing; **f** average vertical mesoscale heat flux for a periodic square wave

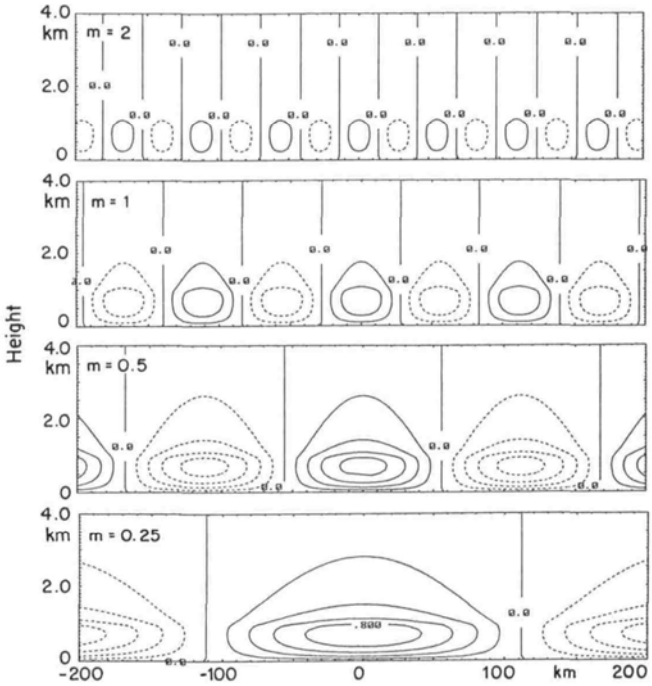

Fig. 5. Mesoscale atmospheric cells for four values of the horizontal wave number for a sinusoidal periodic forcing, $\Delta\psi = 0.2$ (10^3 m^2/s)

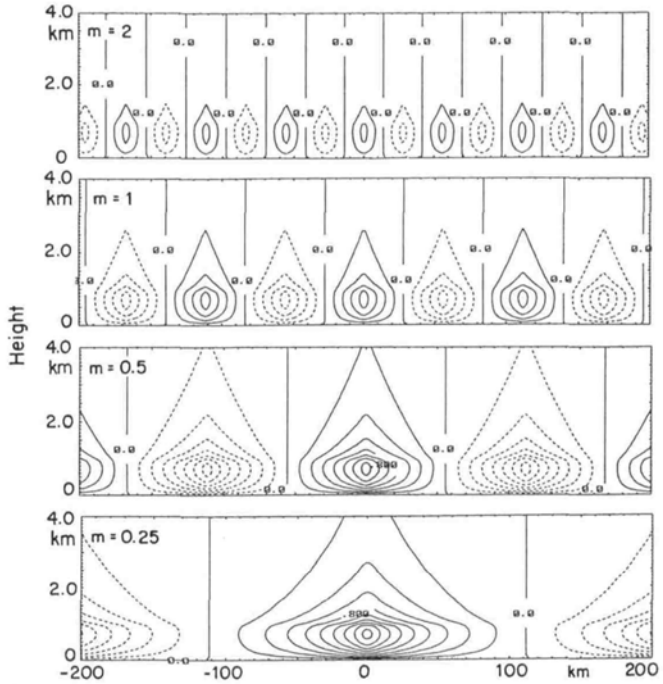

Fig. 6. Mesoscale atmospheric cells for four values of the horizontal wave number for a square wave periodic forcing, $\Delta\psi = 0.2$ (10^3 m^2/s)

when $0.05 < m < 2.2$. The intensity of flow as a function of m for a periodic square forcing is shown in Fig. 4b, and the circulation cells are shown in Fig. 6. In general, the intensity of the flow is larger for a periodic square forcing than for a sinusoidal forcing; the difference is larger at small m. At large m the mesoscale cells interact destructively, reducing the intensity of the flow. The vertical velocity (Fig. 4d) is:

$$w = -\frac{\partial \psi}{\partial x} = w_0\, g(z) \sum_{n=1,3\ldots}^{\infty} \frac{4}{n\pi} \frac{(mn\pi)^2}{(mn\pi)^2+1} \sin\left(\frac{mn\pi x}{R_0}\right), \qquad (36)$$

and the temperature perturbation is:

$$\theta = He(h_0 - z)\left[\frac{1}{2} + \frac{1}{2}\sum_{n=1,3\ldots}^{\infty} \frac{4}{n\pi} \sin\left(\frac{mn\pi x}{R_0}\right)\right] \cdot (h_0 - z)\,\Theta_z - \left\{1 - \frac{He(h_0 - z)}{2}\left[\frac{1}{2} + \frac{1}{2}\sum_{n=1,3\ldots}^{\infty} \frac{4}{n\pi} \cdot \sin\left(\frac{mn\pi x}{R_0}\right)\right]\right\} w\,\Theta_z \frac{t_0}{2}. \qquad (37)$$

Conclusions

Making use of the theory developed by Dalu and Pielke (1989), we study the atmospheric response to spatial gradients of diabatic heat fluxes in the convective boundary layer. Results show that, for sudden changes, the atmospheric perturbation decays exponentially with an *e*-folding distance equal to R_{0_γ}. Square wave periodic surface thermal inhomogeneities generate stronger atmospheric cells than sinusoidally distributed inhomogeneities. The intensity of the flow increases as m increases, reaches its maximum when the wavelength is of the order of R_0, and then decreases linearly for large m. Thus significant atmospheric cells are generated by periodic, thermal inhomogeneous patches only when the wavelength is a significant fraction of R_{0_γ}. It is therefore unnecessary to explicitly resolve in numerical models thermal inhomogeneities on scales much smaller than R_{0_γ} (e.g. as assumed in Avissar and Pielke, 1989). However, since at high m, the vertical velocities are significant and almost constant, mesoscale heat fluxes may be significant; these subgrid-scale effects need to be introduced in parametric form in LAM and GCM, which have only few grid points within a Rossby radius. Solutions for the atmospheric perturbations in the presence of light ambient winds can be derived from the theory presented in this paper, and an extension of our theory in this direction is desirable. When the ambient flow is strong, the pattern of the perturbations is quite different (Hsu, 1987; Robichaud and Lin, 1989); however, the intensity of the mesoscale perturbation is negliglible, since it decays as $1/U^2$.

Acknowledgements. We wish to thank Mike Moran for useful criticism and comments and the reviewers for their help in focusing the paper. We acknowledge the support of the National Science Foundation (NSF) under grant # ATM-8915265, and of the Office of Naval Research, under contract # N00014-88-K-0029. G. A. Dalu, M. Baldi and A. Guerrini acknowledges the support of the ENEL-CNR Project (Rome, Italy). M. Baldi acknowledge the support of NATO through their Scientific Exchange Program. The third Author contribution was supported by the National Science Foundation under Grants ATM-9016562 and EAR-9105059, and by the National Aeronautics and Space Administration.

References

Anthes, R. A., Enhancement of convective precipitation by mesoscale variations in vegetative covering in semiaride regions, *J. Appl. Meteorol.* **23,** 541–554, 1984.

Abbs, D. J., and R. A. Pielke, Thermally forced surface flow and convergence patterns over northeast Colorado, *Mon. Weather Rev.*, **14,** 2281–2296, 1986.

Avissar, R., and R. A. Pielke, A parameterization of land heterogeneous land surfaces for atmospheric numerical models and its impact on regional meteorology, *Mon. Weather Rev.*, **117,** 2113–2136, 1989.

Dalu, G. A., and R. A. Pielke, An analytical study of the sea breeze, *J. Atmos. Sci.*, **46,** 1815–1825, 1989.

Fodor, G., *Laplace Transform in Engineering,* Hungarian Academy of Science, Budapest, 1965.

Garrett, A. J., A parameter study of interactions between convective clouds, the convective boundary layer, and forested surface, *Mon. Weather Rev.*, **110,** 1041–1059, 1982.

Green, J. A. S., and G. A. Dalu, Mesoscale energy generated in the boundary layer, *Q. J. Roy. Meteorol. Soc.*, **106,** 721–726, 1980.

Hanna, S. R., and S. D. Swisher, Meteorological effects of the heat and moisture produced by man, *Nucl. Saf.*, **12,** 114–122, 1971.

Hsu, H.-M., Study of linear steady atmospheric flow above a finite surface heating, *J. Atmos. Sci.*, **44,** 186–199, 1987.

Mahfouf, J-F., E. Richard and P. Mascart, The influence of soil and vegetation on the development of mesoscale circulations, *J. Clim. Appl. Meteorol.*, **26,** 1483–1495, 1987.

Mahrer, Y., and R. A. Pielke, A numerical study of the air flow over irregular terrain, *Contrib. Atmos. Phys.*, **50,** 98–113, 1977.

McCumber, M. C., and R. A. Pielke, Simulation of the effects of surface fluxes of heat and moisture in a mesoscale numerical model, *J. Geophys. Res.*, **86,** 9929–9938, 1981.

Pielke, R. A., *Mesoscale Meteorological Modeling,* Academic Press, New York, N.Y., 1984.

Pielke, R. A., and M. Segal, Mesoscale circulations forced by differential terrain heating in: *Mesoscale Meteorology and Forecasting,* Ed. P. S. Ray, Am. Meteorol. Soc., Boston, Mass., 1986.

Pielke, R. A., G. A. Dalu, J. S. Snook, T. J. Lee, and T. G. F. Kittel, Nonlinear influence of mesoscale land use on weather and climate, *J. Clim.*, in press, 1991.

Robichaud, A., and C. A. Lin, Simple models of diabatically forced mesoscale circulations and mechanism of amplification, *J. Geophys. Res.*, **94,** 3413–3426, 1989.

Rotunno, R., On the linear theory of land and sea breeze, *J. Atmos. Sci.*, **40,** 1999–2009, 1983.

Segal, M., R. A. Pielke, and Y. Mahrer, Evaluation of surface sensible heat flux effects on the generation and modification of mesoscale circulation, *Proc. Second Int. Symp. on Nowcasting,* European Space Agency, Norrkoping, Sweden, 263–269, 1984.

Segal, M., R. Avissar, M. C. McCumber, and R. A. Pielke, Evaluation of vegetation effects on the generation and modification of mesoscale circulations, *J. Atmos. Sci.*, **45,** 2268–2292, 1988.

Segal, M., W. E. Schriber, G. Kallos, J. R. Garrat, A. Rodi, J. Weaver and R. A. Pielke, The impact of crop areas in Northern Colorado on midsummer mesoscale thermal circulations, *Mon. Weather Rev.*, **107,** 809–825, 1989.

Sun, W., and I. Orlanski, Large mesoscale convection and sea breeze circulation. Part I: linear stability analysis, *J. Atmos. Sci.*, **38,** 1675–1693, 1981.

Yan, H., and R. A. Anthes, The effect of variations in surface on mesoscale circulations, *Mon. Weather Rev.*, **116,** 192–208, 1988.

Wezel, P. J., and J. T. Chang, Evapotranspiration from non-uniform surfaces: A first approach for short-term numerical weather prediction, *Mon. Wheater Rev.*, **116,** 600–621, 1988.

Zhang, D., and R. A. Anthes, A high-resolution model of the planetary boundary layer-sensitivity tests and comparisons with SESAME-79 data, *J. Appl. Meteorol.* **21,** 1594–1609, 1982.